



Pesticide abatement using environmentally friendly nano zero valent particles as photo-Fenton catalyst

A.M. Díez^{a,b,*}, Manuela M. Moreira^a, M. Pazos^b, M.A. Sanromán^b, T. Albergaria^a, C. Delerue-Matos^a

^a REQUIMTE/LAQV, Instituto Superior de Engenharia do Porto, Instituto Politécnico do Porto, Rua Dr. António Bernardino de Almeida, 431, 4200-072 Porto, Portugal

^b CINTECX, Universidade de Vigo, BIOSUV Group, Department of Chemical Engineering, 36310 Vigo, Spain

ARTICLE INFO

Editor: Jorge Bedia

Keywords:

Circular economy
Emerging pollutant degradation
Real wastewater remediation
Visible radiation
Deep characterization techniques

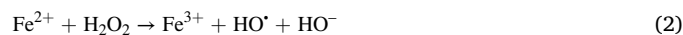
ABSTRACT

Nano-zero valent iron particles (NZVI) have been used for the pesticide pirimicarb degradation under simulated solar radiation. These particles have been synthesized by extracts from agro-industrial residues, namely vineyard and blueberry pruning, black tea and algae, so they can be labelled as “green-NZVI”. The physico-chemical properties of these green-NZVI were compared to those of NZVI synthesized with NaBH₄. The usage of agro-industrial residues as reducing agent not only provided better performant NZVI but also evaded the usage of harmful reagents. Indeed, this process is not only within circular economy, and environmentally friendly, but also defeats the degradation performance of the widely reported photo-Fenton process with Fe²⁺ catalyst. 96.5 % pirimicarb degradation was achieved under simulated solar radiation within 15 min with 0.08 mM H₂O₂ and 0.16 mM NZVI synthesized with black tea extract. Further, the developed process was optimized in terms of reagents concentration and natural antioxidant extract used for NZVI synthesis, which demonstrated a strong effect on pirimicarb degradation due to the differences on natural phenolic compounds present on them. The pirimicarb degradation pathway was analysed, confirming the successful pesticide degradation. In terms of H₂O₂ concentration, it can be reduced by its sequential addition in time. Under optimal conditions, even real effluents can be successfully degraded.

1. Introduction

Nano-zero valent particles (NZV), specifically of iron (NZVI), have been receiving a lot of attention as an easy and non-selective agent for eliminating organic matter [1,2] due to a series of oxidation and reduction reactions. These reactions make the usage of NZVI to be labelled as an Advanced Oxidation Process (AOPs). Indeed, NZVI have demonstrated activity on the self-generation of hydroxyl radicals (HO[•]), which attack quickly and non-selectively the organic matter. This happens by the natural behaviour of NZVI in an oxygenated environment (Eq. (1)) [2] where NZVI generate the Fenton reagents and consequently, the Fenton reaction occurs (Eq. (2)) [3]. Thus, NZVI act as a continuous supplier of the Fenton catalyst (Fe²⁺) (Eq. (1)), allowing the achievement of similar rates of degradation when compared to homogeneous Fenton processes [1], without any of its disadvantages including environmental concerns and experimental difficulties such as the excessive iron content which is related to sludge generation and iron

hydroxides precipitation [4]. Meanwhile, NZVI can gradually supply Fe²⁺ for the Fenton process, serving as an additional degradation mechanism and after the treatment, they can be eliminated from the bulb solution and even reused [2,4]. However, some of the self-generated H₂O₂ can react with Fe⁰ (NZVI) (Eq. (3)) working as a supplier of Fe²⁺, but leading to H₂O₂ diminution [5]. This is why some authors have explored the alternative of adding additional H₂O₂ [2,5,6].



Moreover, the addition of radiation can enhance the process performance due to (i) the direct photolysis of the target pollutant or its by-products, (ii) the homolytic breakage of H₂O₂ (attained by UVC radiation) [6], (iii) the regeneration of Fe²⁺ from the spent Fe³⁺ (produced during the Fenton process, Eq. (2) which leads to both HO[•] generation

* Corresponding author.

E-mail address: adiez@uvigo.gal (A.M. Díez).

and Fe^{2+} constant supply (photo-Fenton process) (Eq. (4) [7] and iv) the breakage of the iron complexes with both organic matter or hydroxides which may be formed throughout the Fenton process [3].



However, NZV are usually synthesized by the reduction of the corresponding cations by using harmful chemicals, such as NaBH_4 [2,8] which generates toxic, corrosive (BO_3^3) and explosive (H_2) compounds [9]. Other approach for NVI synthesis is based on calcination processes under N_2 atmosphere [10], which is an expensive and complex process

for practical applications. The usage of antioxidant extracts, prepared from agro-industrial residues, for the reduction of metal salts to produce NZV is proposed as an economic, quick and environmentally friendly solution [9]. Thus, the synthesis of NZVI becomes more viable, and simultaneously, agro-industrial residues are revalorized. This aligns with the principles of circular economy and prevents the accumulation of these residues on large areas of land that could be used for more profitable objectives. Indeed, other authors have tested the utilization of tree leaves extracts [11], mango peel extracts [12] or grape leaves extracts [13]. Nevertheless, NZVI have been mainly used for the

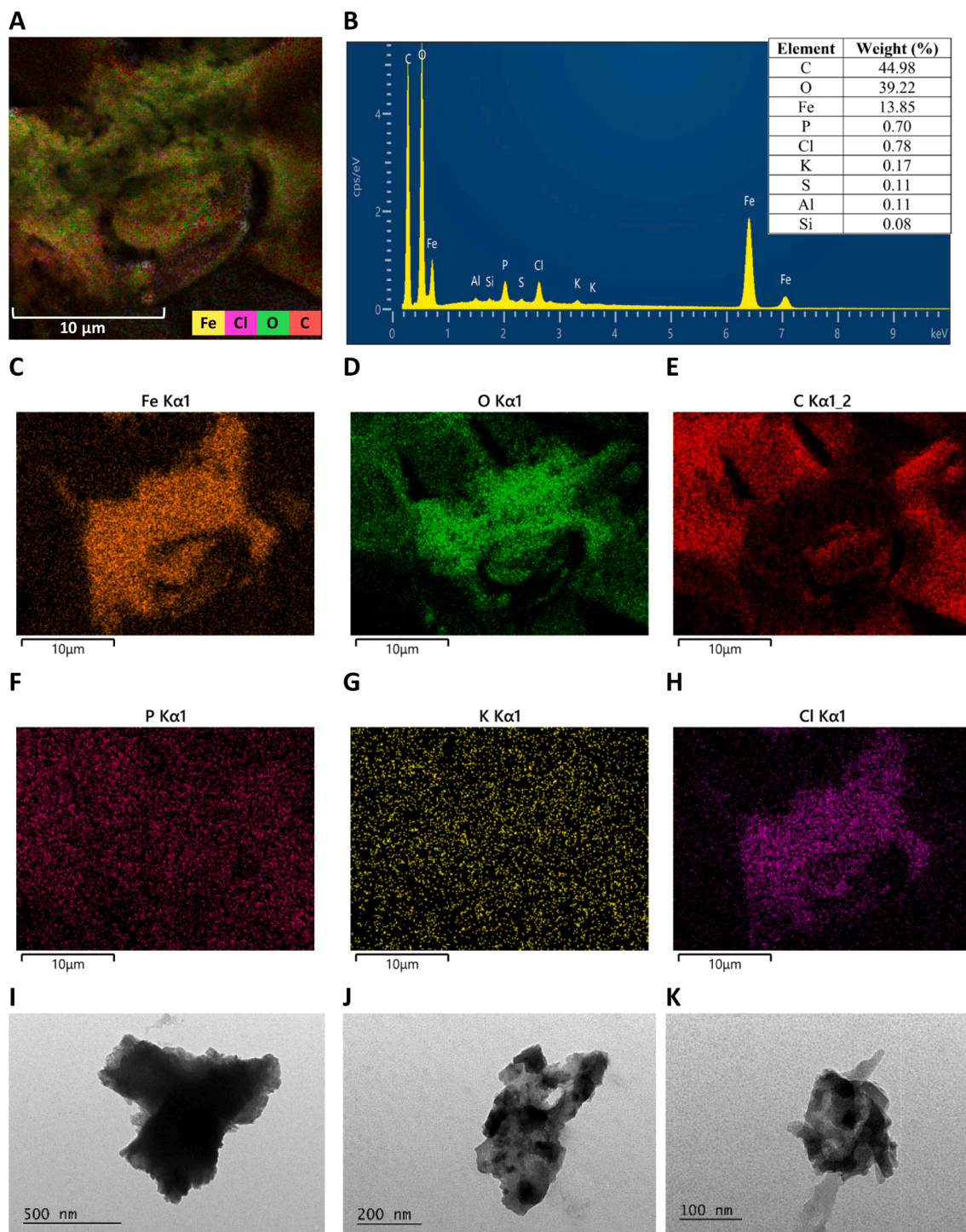


Fig. 1. SEM image of NZVI with element distribution (A) and EDS results (B). Element SEM images (C–H). TEM images with x15,000 (I), x25,000 (J) and x50,000 (K).

degradation of dyes [12,14] or metals [9] and have never been used for pirimicarb degradation although this pesticide is extensively used [15].

Thus, to test the performance of the above-mentioned processes, pirimicarb pesticide was used as model pollutant. Pesticides degradation is an issue of high priority due to their stable structure even under adverse environmental conditions, indeed, they are persistent, possess elevated toxicity (they are meant to fight against live organisms) and they are highly manufactured (they are used for coping with the extensive food demand) [7].

The aim of this research is to study the NZVI activity under simulated solar radiation, which has been poorly studied (Fig. 1-SM: Supplementary Material). The effect of different parameters, such as H₂O₂ addition, catalysts dosage, treatment time and matrix influence, was studied in order to attain an efficient pirimicarb degradation. What is more, the unreported characterization and comparison of the reduction activity of different agro-industrial residues for NZVI generation has been assessed. The attained particles showed different physico-chemical properties than those synthesized by traditional NaBH₄. The green-NZVI showed different performance on pirimicarb degradation due to the organic compounds present of those extracts, which are consequently determined. The degradation mechanism was deeply studied, by analysing pirimicarb by-products generation and scavengers' experiences. Finally, the treatment of a real wastewater and NZVI reuse was accomplished.

2. Materials and methods

2.1. Reagents and samples

Pirimicarb analytical standard (99.6 %) and FeCl₃·6H₂O (98 %), 7-hydroxicoumarin were acquired from Sigma-Aldrich were purchased from Sigma-Aldrich and H₂O₂ (30 %) was bought to LabChem. Scavenger reagents, namely 2,2,6,6-tetramethylpiperidin-1-yl) oxidanyl: TEMPO, sodium azide, coumarin and ethylenediamine tetraacetic acid: EDTA (all of them 99 %) were acquired from Sigma-Aldrich. Milli-Q water was attained from Millipore purification system (18.2 mΩ·cm resistivity). The black tea was purchased from Tetley®, the brown (*Fucus spiralis*) and green (*Ulva* spp.) algae were collected from Porto beaches and vineyard and blueberry pruning were donated from local producers (Porto, Portugal).

2.2. NZVI synthesis

The NZVI were synthesized by the reduction of iron cations with the natural antioxidant extract. The antioxidant extracts were prepared by the addition of 2 g of the selected material into 100 mL of deionized water. This mixture was placed in a shaker at 80 °C for 20 min, filtered and stored in darkness conditions up to three days.

On the other hand, a FeCl₃ solution 0.1 M was prepared. The quantity of the antioxidant extract required for NZVI synthesis depends on its nature. For instance, and as starting point, to synthesize NZVI, 1 mL of the black tea extract was added for each 0.004 mmol of iron (40 μL of FeCl₃ solution (0.1 M)). This synthesis was done directly on the reactor vials, so once the particles are generated, the degradation process starts.

For comparison aims, NZVI were also synthesized by the typical addition of NaBH₄. For that, a 0.5 M NaBH₄ solution was done on NaOH 0.1 M at 5 °C, in order to maintain NaBH₄ stability, avoiding H₂ liberation. This solution was replaced as soon as bubbles were noticed on the containing bottle. For the NZVI synthesis, the ratio 40 μL FeCl₃ 0.1 M:100 μL NaBH₄ solution was kept, maintaining, approximately the addition of 10 times more NaBH₄ to ensure proper Fe⁺³ reduction [16].

2.3. Degradation set-up

11 mg/L of pirimicarb was used as the model working solution. The degradation experiences were done on 40 mL reactor vials where 25 mL of a solution of pirimicarb, FeCl₃, antioxidant extract and H₂O₂ were

added (further explanations on SM). The glassy reactor vials (2.7 cm diameter × 7 cm high, 40 mL of capacity) were closed with silicone taps which allowed a slight volume modification as gases may be generated through the degradation process and evaporation can occur, due to temperature increase. The tubes were placed in aluminium foil, used as flat parabolic collector and the radiation was given by a solar simulation lamp (400–740 nm, 600 W from Toplanet) which was placed at 10 cm from the glass tubes (Fig. 2-SM).

Validation experiences were done using as working matrix tap water and real wastewaters from a Wastewater Treatment Plant (Tui, Guil-lareí). Thus, primary (physically treated) and secondary (physical and biologically treated) wastewaters were used as matrix, and their characterization is shown in Table 1-SM.

2.4. Analysis

2.4.1. NZVI characterization

SEM and EDS were measured using JEOL JSM6010LA equipment. TEM spectra was made with the electronic microscope JEOL JEM1010 (200 kv) (CACTI, University of Vigo).

Fourier transform infrared spectroscopy (FTIR) was attained using the FTIR Nicolet-6700 (Thermo) whereas Raman was measured with Horiba Jobin Yvon HR800UV spectrophotometer (633 nm). X-Ray Diffraction spectroscopy (XRD) was measured using the X'Pert Pro (PANalytical) diffractometer (CACTI, University of Vigo).

UV-Vis spectra was measured using the spectrophotometer. With that, Tauc relation (Eq. (5)) was used for calculating band gap of NZVI. Where α is the adsorption coefficient, h is Planck constant, V is the light intensity and E_g is the band gap [17].

$$(\alpha h\nu)^{1/2} = C(h\nu - E_g) \quad (5)$$

The electrochemical characterization was done using Nova Autolab (Metrohm) equipment. For that, an electrochemical cell of 100 mL of NaOH 1 M was used. Using Pt wire as counter electrode, HgCl₂ as reference electrode, and Ni foam (1 cm²) as working electrode where 0.25 mg NZVP were deposited. The deposition was made from a dispersion of NZVP (0.5 mg) in EtOH (500 μL) and Nafion (30 μL). This mixture was homogenized by an ultrasonic probe (Bandelin Sonopuls) and drop-deposited (515 μL) on Ni foam. Under this conditions, Cyclic Voltammetries (CV) and Electrochemical Impedance Spectroscopy (EIS), with the attainment of Nyquist graphs, were attained.

Inductive Coupled Plasma (ICP) using the Agilent Technologies series AA (CACTI, University of Vigo) was used for measuring the iron leaching after the degradation process. The pH of point of zero charge (pH_{PZC}) was measured following a modified previous procedure [18]. Thus, 5 beakers were prepared with 10 mL on NaNO₃ 0.1 M at different initial pH by the adjustment with NaOH or HNO₃. In each beaker, 20 mg of NZVI were added and the system was left 24 h under magnetic stirring (600 rpm). After that, the pH was measured and the representation of initial pH vs. pH variation provided a line where the pH_{PZC} was attained by the interception of this line on the x axis.

2.4.2. Pirimicarb measurement

The chromatographic separation was achieved using the HPLC-DAD Agilent 1260 with a Luna C₁₈ column (150 mm × 4.6 mm, 5 μm) from Phenomenex (30 °C) using a previous method [19] with slight modifications detailed on SM.

2.5. Process evaluation

2.5.1. Process selection

To begin with, a comparison of the pirimicarb degradation under different photo-based conditions was carried out. For that, traditional photolysis and photo-Fenton (H₂O₂ + Fe²⁺) processes were assessed. Moreover, photo-Fenton-NZVI was evaluated, that is the photo-Fenton

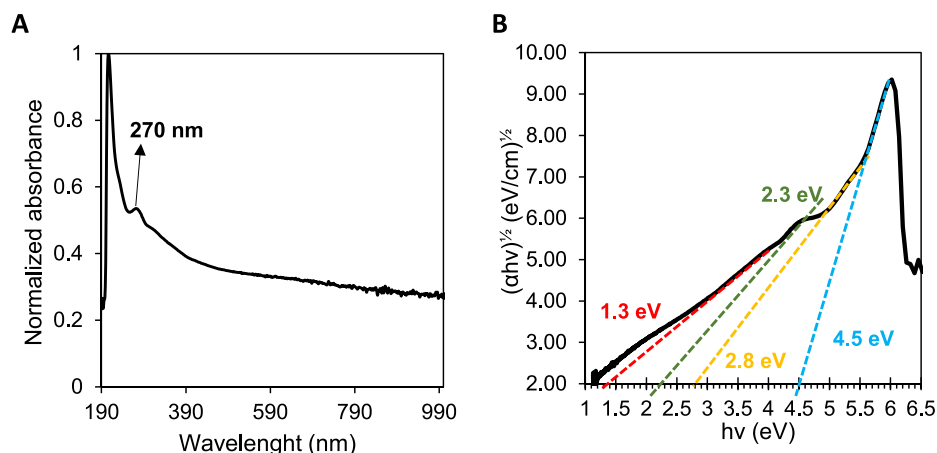


Fig. 2. Absorbance spectra of NZVI (A) and Tauc plot (B).

process using NZVI of iron source instead of Fe^{2+} . For the synthesis of NZVI, tea extract was added, and consequently, its influence on degradation was independently assessed, as well as that of H_2O_2 and the combination of tea extract with H_2O_2 . Moreover, the performance of NZVI under radiation was also tested (without H_2O_2 addition). Moreover, the photoactivity of “old NZVI” was tested, that is NZVI which were synthesized, filtered and stored instead of synthesized *in situ* on the reactor tubes as aforementioned described (Section 2.2). Out of the optimal process, the comparison of the pirimicarb degradation under darkness conditions was also made.

2.5.2. Process optimization

H_2O_2 concentration effect was studied (0.005–0.08 mM) fixing NZVI concentration at 0.16 mM). Likewise, NZVI concentration was optimized (0.04–2.88 mM) keeping H_2O_2 concentration at 0.02 mM. Subsequently, the NZVI synthesis process was studied with different agro-industrial residues, by optimizing the required volume of extract for achieving complete Fe^{3+} reduction using the spectrophotometer (Thermo Scientific, evolution 300) and measuring the extract colour change at 596 nm. The augmentation on absorbance is directly related to NZVI generation (black colour). Therefore, when the absorbance starts to decay, is the point where no more NZVI are generated and the iron solution (yellowish) only dilutes the black colour (NZVI concentration). Then, the NZVI synthesized with various extracts were used for pirimicarb degradation under the optimal conditions on terms of H_2O_2 and NZVI concentration.

2.5.3. Extracts phenolic content and antioxidant activity characterization

In order to understand the attained results and to explain the degradation capability of the NZVI synthesized with different agro-industrial residues extracts, a deep characterization was done as described in detail by Moreira et al. [20]. Thus, the antioxidant activity and the phenolic composition of the extracts prepared from the agro-food wastes were characterized by different spectrophotometric and chromatographic assays (SM).

2.5.4. Degradation mechanisms

2.5.4.1. Scavenger experiences. To understand the generation of oxidant species throughout the treatment, scavenger experiences were done. For that, 2 mM of TEMPO, sodium azide, coumarin or EDTA were added to the reactor vials in order to quench different reactive species. The observed reduction in degradation performance compared to experiments without scavenger addition is directly related to the influence of the scavenged substance on the degradation process [21].

2.5.4.2. Hydroxyl radical generation. HO^\bullet generation was measured by mixing 200 μL sample with 2 mL solution of coumarin (2 mM) which reacts with 29 % of the produced HO^\bullet , producing 7-hydroxicoumarin which exhibits fluorescence at a wavelength of 455 nm [22]. This fluorescence emission was measured using the Jasco FP-8300 fluorimeter. By establishing a calibration curve, it was possible to determine the concentration of HO^\bullet in the reaction mixture.

To achieve this, degradation experiments were conducted by replicating the experimental set-up, but replacing the pirimicarb solution with deionized water. Consequently, the addition of the antioxidant extract along with FeCl_3 0.1 M solution facilitated the *in situ* synthesis of the desired NZVI. These NZVI generated HO^\bullet themselves, and samples were collected at regular intervals to assess the concentration of them over time.

2.5.4.3. By-products. The generated by-products were measured at CACTI on University of Vigo with the HPLC-MS (Hewlett-Packard 5989B) with a ZORBAX Eclipse XDB-C18 column (Agilent), flowing the procedure detailed on SM.

3. Results and discussion

3.1. NZVI characterization

3.1.1. FTIR

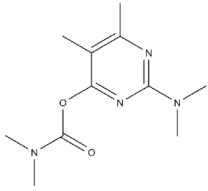
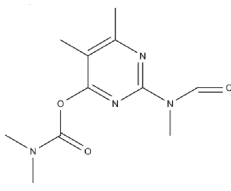
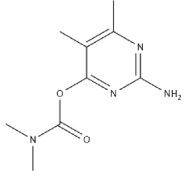
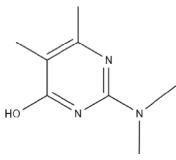
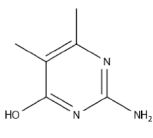
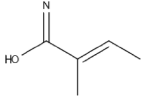
The generation of radicals by NZVI is noticed on FTIR spectra (Fig. 3-SM-A), where the peaks between $3,700$ and $2,500\text{ cm}^{-1}$ are caused by the stretching of the formed H-O bonds [13]. Moreover, the signal between 400 and 800 cm^{-1} has been related to Fe-O stretching on Fe_3O_4 which intensity is diminished by the presence of organic molecules from the green NZVI synthesis [14]. At 1630 cm^{-1} a peak related to adsorbed water is found [1]. The remaining tea extracts can be detected on C=O and C-OH bonds appearing at, respectively, $1,681$ and $1,061\text{ cm}^{-1}$.

3.1.2. SEM and TEM

SEM images (Fig. 1) demonstrate the successful synthesis of NZVI, where a structure of Fe is formed within the remaining organic content of the reducing agent. Moreover, oxygen can be clearly detected, demonstrating HO^\bullet were formed and ended up by forming HO– bonds. P and Cl are also detected due to the usage of the natural extract and FeCl_3 as precursors. Moreover, the homogeneous distribution of the elements (Fig. 1-C:H) indicates a successful synthesis.

Regarding TEM images (Fig. 1-I:K), particle size is around 200–500 nm, due to agglomeration which is common in NZVI [23] and favours their separation from the treated effluent, working as a heterogeneous catalyst. The attained NZVI showed amorphous shape which may be due

Table 1
Pirimicarb intermediates analysed during the photo-Fenton-NZVI treatment.

Compound	Structure	Main peaks (m/z)	Reference
I		137 195, 239	This study, [15,35]
II		275	This study, [50]
III		154, 166	This study, [15]
IV		123, 98, 72	This study, [33,65]
V		123, 140	This study, [15]
VI		98	This study, [66]

to the quick synthesis process and the fact oxygen bounds metal oxides, forming more nucleation sites [14]. Indeed, other authors have presented spherical structures after NZVI synthesis with NaBH_4 because of this being a slower synthesis process. These amorphous structures can promote more easily the degradation process due to a higher available surface area (although BET is almost insignificant on NZVI [24]).

3.1.3. XRD

XRD results demonstrate the non-crystalline structure of NZVI (Fig. 3-SM-B) which may be explained by the rapid synthesis process and the presence of an heterogeneous organic content on the antioxidant extract [24]. Indeed, it has been reported the obtaining of amorphous XRD profile for green-synthesized NZVI [11,24].

3.1.4. Band gap

The UV-Vis spectrum of NZVI was measured (Fig. 2-A) where one can detect the small peak at 270 nm which is characteristic of NZVI [8]. It can be seen on the normalized absorbance spectrum how even though maximum absorbance peaks are placed at the UV range, visible signal do not drop under 30 %, meaning NZVI keep adsorbing on the visible range, which make them to be also activated under visible radiation. Indeed, applying Tauc formula (Eq. (5)), different band gaps were calculated, between 1.3 and 4.5 eV (Fig. 2-B). This defeats previous data on NZVI performance where visible adsorption was negligible [12] or where unique band gaps were attained [17]. Thus, the green and quick synthesis hereby proposed may promote an enhancement when compared to these previous studies where NaBH_4 was used as reduction agent. This is in concordance with other authors who have reported the presence of multiple band gaps on structures with defects [25] which is related to a quick synthesis process and the presence of different organic molecules.

3.1.5. Electrochemical characterization

Latest studies have previously presented electrochemical studies for the characterization of NZVP. For instance, Arularasu et al. [14] used EIS to characterize green synthesized NZVI and Pirsasheb et al. [26] have measured CVs of their NZVI, as the electrochemical behaviour indicates the suitability of this catalyst to be used as a degradation tool [14].

CV results are shown on Fig. 3-A where a pre-oxidation peak appears at 1.55 V, demonstrating some H^+ accumulation takes place, although at high potentials, leaving the degradation pathway as the spontaneous reaction [27]. Indeed, it can be seen how a pre-reduction peak appears at 1.48 V, demonstrating those particles act as highly reductive catalysts [26]. Tafel slope is related to the speed of the reduction reactions, the small value attained demonstrates a high current response for a given potential [28], indicating a good electron transfer [29]. Fig. 3-B demonstrates NZVI provide a unique arc on the Nyquist plot, establishing a single relaxation process is happening with an increase on the boundary resistance, caused by oxygen adsorption on the n-type conductivity surface [14].

3.1.6. Point of zero charge

The pH_{PZC} of NZVI resulted 3.89 (Fig. 4-SM). Usually, this type of particles possesses a neutral pH. In this case, the acidification of the structure can be caused by the presence of organic acids on the black tea extract (section 3.2.2.3).

3.2. Process evaluation

3.2.1. Process selection

The comparison of several photo degradation processes was carried out. Initially, the simulated solar degradation of pirimicarb was tested and it was undetectable during 15 h. Then, several NZVI experiences and its controls were carried out (Fig. 4) fixing NZVI at 0.16 mM and H_2O_2 at 0.08 mM, if added.

The synergistic combination of NZVI and photolysis was evaluated. For that, the previously used black tea extract was employed as reduction agent of the FeCl_3 . As it can be seen, NZVI caused 23 % pirimicarb degradation thanks to the self-generation of HO^\bullet (section 3.2.5.2). H_2O_2 addition increased pirimicarb degradation from 23 % to 97 %. This can be explained by the Fenton process (that is the reaction between Fe^{2+} and H_2O_2 which produces HO^\bullet which degrade organic matter [3]) or due to Fe^0 (NZVI) which also promote Fenton-like reactions [1]. This process would be named photo-Fenton-NZVI ($\text{NZVI} + \text{H}_2\text{O}_2$ on Fig. 4).

To understand the influence on pirimicarb degradation of H_2O_2 and black tea extract, their individual effect was also evaluated. As it can be seen on Fig. 4, photo- H_2O_2 caused around 35 % degradation due to the generation of some radicals with radiation, as it has been reported that H_2O_2 self-decomposition does not generate radicals [1]. The addition of the black tea extract led to 9.5 % pirimicarb degradation (Fig. 4), which may be caused by the presence of some photoactive organic

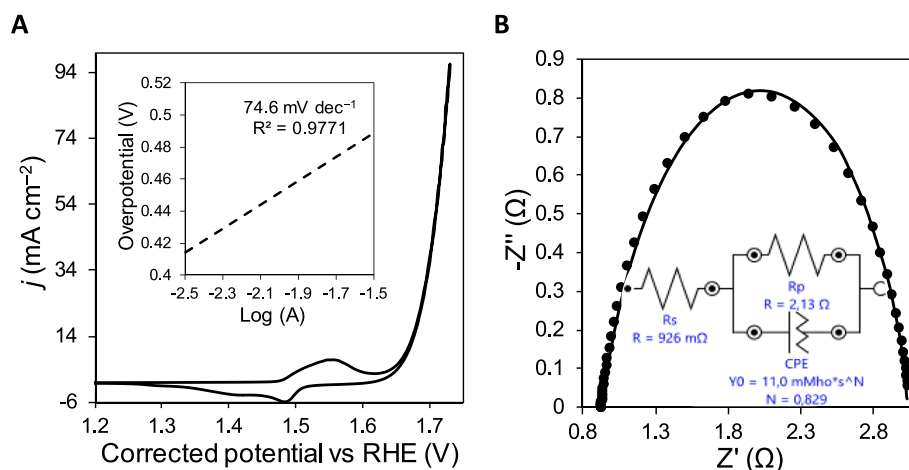


Fig. 3. NZVI response to CV studies (A) with Tafel slope measurement (embedded graph) and to EIS measurement (B).

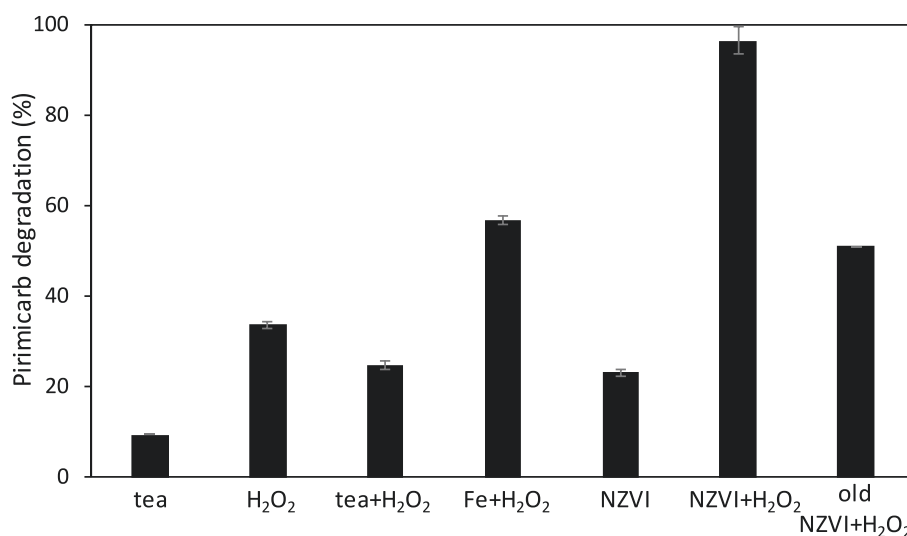


Fig. 4. Pirimicarb degradation after 15 min under simulated solar radiation with 0.16 mM Fe, 0.08 mM H₂O₂ and 1 mL of black tea extract on the required experiences.

compounds which generate oxidant species (section 3.2.2.3). The combination of both black tea extract and H₂O₂ led to 24.7 % pirimicarb degradation indicating a 10 % detriment when compared to H₂O₂ alone (Fig. 4). This can be caused by the antioxidant behaviour exhibited by the compounds present on black tea extract [30], acting as H₂O₂ scavenger.

The NZVI synthesis is immediate and usually it is made on the bulk solution (so-called *in situ*). However, the approach of synthesizing the particles separately (*ex situ*) and adding them to the pirimicarb solution (so-called “old NZVI” in Fig. 4) was also tested with the addition of H₂O₂. This approach results in a pirimicarb degradation reduction of around 40 %, demonstrating that the direct *in situ* synthesis is not only easier to apply, but also more effective. This is related to the fast self-oxidation of NZVI, and thus, synthesis and application should be as close as possible [31].

Moreover, the obtained results were also compared with the typical homogeneous photo-Fenton process (labelled Fe + H₂O₂ on Fig. 4). As it can be observed, the pirimicarb degradation only reached 56 %, highlighting the fact Fe²⁺ is converted to Fe³⁺ which results in the Fenton process performance to drop [3] when compared to photo-Fenton-NZVI.

Taking into consideration the obtained results, the best performance was attained with photo-Fenton-NZVI. This process has the potential of degrading almost completely (96.5 %) pirimicarb within 15 min. This

process was compared to dark Fenton-NZVI (Fig. 5-SM-A), confirming the powerfulness of this solar-photo-Fenton-NZVI process. Under darkness conditions, the degradation reached a maximum 60 % degradation after 10 min. This can be caused by an excess of Fe³⁺ and Fe hydroxides which could be, respectively, regenerated and broken by radiation [3,7] on the photo-Fenton-NZVI process. Indeed, other authors have demonstrated the degradation enhancement of the photo-Fenton-NZVI process when compared to Fenton-NZVI. Thus, dark Fenton usually gets to steady degradation rates (Fig. 5-SM) [32] due to the disappearance of H₂O₂ and Fe²⁺ as time passes, caused by H₂O₂ conversion into HO[•] and HO⁻ through the Fenton reaction and the generation of Fe hydroxides and organic complexes [4,6]. Indeed, a previous study carried out by Bao et al. [16] demonstrated the Fenton degradation with NZVI was initially fast and then the degradation was slower, due to the limitation of the Fenton reagents. Those results are in concordance with the kinetic studies made (Fig. 5-SM-B), where Fenton-NZVI process showed two kinetics trends whereas photo-Fenton-NZVI process reported a constant degradation increase. There, pseudo-first order kinetic model fitted well the data, due to the effect of HO[•] concentration on the degradation process [33]. The kinetic constants (table 2-SM) highlight the initial (2.5 min) faster pirimicarb degradation of the Fenton-NZVI process. This higher degradation rate when compared to photo-Fenton-NZVI can be caused by the H₂O₂ or NZVI decomposition under radiation application.

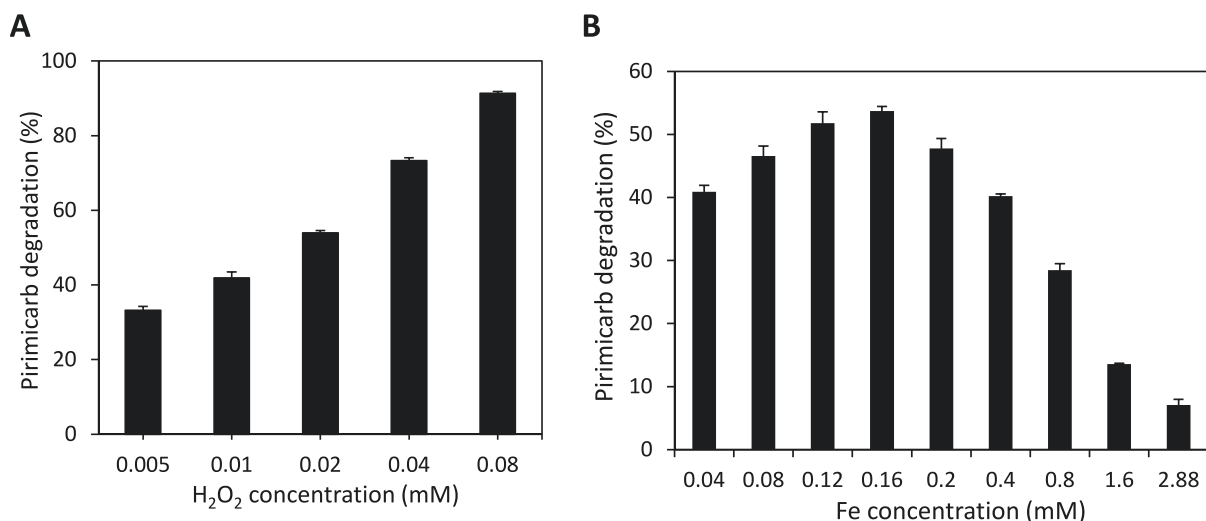


Fig. 5. Pirimicarb degradation after 15 min under simulated solar radiation A: with 0.16 mM Fe and different H₂O₂ concentrations or B: with 0.02 mM H₂O₂ and different Fe concentrations.

Nevertheless, Fenton-NZVI process achieved, after the initial 2.5 min, a steady degradation rate, whereas solar radiation on the photo-Fenton-NZVI keep the process going due to NZVI activation and Fe complexes breakage [3].

3.2.2. Process optimization

3.2.2.1. H₂O₂ concentration. Photo-Fenton-NZVI process was consequently selected as the optimal process. Then, H₂O₂ concentration effect was studied, which was varied between 0.005 and 0.08 mM. With this, the process was optimized working at H₂O₂ concentrations far below those previously reported [36–38]. As noticed on Fig. 5-A, the increase on H₂O₂ concentration led to a higher pirimicarb degradation, due to its direct relationship with HO[•] generation [39]. H₂O₂ is an unstable and explosive reagent, difficult to storage and transport [40] which utilization is mean to be reduced; therefore, H₂O₂ concentrations higher than 0.08 mM were not even assessed. Considering this and the high catalytic behaviour of NZVI [2], in the present study, 0.02 mM was set as working H₂O₂ concentration to avoid an excess of it and to have the opportunity of optimizing the process by other means.

H₂O₂ addition enhances the process due to the initial radical's generation. Moreover, the remaining iron on the solution can lead to the photo-Fenton process. Indeed, Tsai et al. [34] tested the 10 mg/L pirimicarb degradation under simulated visible radiation (similar conditions to this study) without H₂O₂ addition by using Pt/AgInS₂ and they needed 24 h to attain almost complete pirimicarb degradation. Thus, even though H₂O₂ usage should be reduced, the addition of 0.08 mM in this research enabled to reduce the pirimicarb degradation time to 15 min. This is in concordance with Vidot et al. [41] who defended the importance of the iron content stating that using three times Fe²⁺ concentration with regard to H₂O₂ concentration ensures the complete conversion of the latter into HO[•] during the Fenton reaction.

3.2.2.2. NZVI concentration. NZVI concentration effect was evaluated from 0.04 to 2.88 mM at 0.02 mM of H₂O₂. These concentrations were also far below the NZVI concentrations used on degradation processes [38,42], reducing then the iron leaching below 0.11 ng/L. According to the results expressed in Fig. 5-B, increasing the NZVI concentration from 0.04 to 0.16 mM caused a gradual 24 % enhancement on pirimicarb degradation, which can be explained by the augmentation of active sites [43] and the possibility of decomposing more H₂O₂ into HO[•] [2]. These results are in concordance with Li et al. [39] who also detected a 12 % increase on 2,4-dichlorophenol degradation when augmenting 4 times

the NZVI dosage. These authors highlighted how the higher amount of NZVI favoured the HO[•] generation. However, increasing the iron concentration from 0.16 to 2.88 mM, led to a pirimicarb degradation reduction of 85 %. This phenomenon can be explained by an excess of catalyst which not only led to radiation scattering but also to NZVI agglomeration causing a limitation on mass transfer [43].

Moreover, taking into account that H₂O₂ is being added, the effect of the photo-Fenton process should also be considered as it has been reported that high iron concentrations lead to competitive reactions with H₂O₂, diminishing the degradation performance [44]. Another drawback of an excess of iron concentration is related to the fact that HO[•] can be consumed by the excess of NZVI [2].

Additionally, the use of lower iron concentrations favours the antioxidant compounds present on black tea extract to behave as pro-oxidants, and in the case of high iron concentrations, the iron chelation and antioxidant behaviour of the extract is more evident [41]. This can be explained by the fact that some chelants of Fe⁺ and Fe³⁺ favour the Fe²⁺ presence and others its solubilisation [45]. Demir-Duz et al. [44] worked with a slightly higher iron concentration (10 mg/L = 0.17 mM) and considered their degradation process to be green enough to be applied in the future. Likewise, Yu et al. [46] used much more NZVI (approximately 6 mM NZVI = 0.35 g/L) for achieving 99.38 % degradation of the pesticide. Their process took half an hour, demonstrating a slower degradation rate which may be caused by the NZVI being trapped on biochar, or the usage of NaBH₄ as reducing agent, causing structural NZVI modifications and impeding the pro-oxidants of the natural extracts used in this study. Consequently, the hereby selected optimal iron concentration (0.16 mM) is low enough to be fitted into the zero-discharge concept. Nevertheless, NZVI can be separated through filtration or centrifugation avoiding the drawbacks of working in homogeneous mode, although the degradation performance is comparable.

Even though 0.16 mM of NZVI was selected as optimal working concentration, tests with the higher iron concentration were done in order to know if naturally iron polluted effluents, such as the ones coming from the steel company [47] or mines [48] could be used for NZVI synthesis and subsequent degradation processes. Indeed, the process performance with 2.88 mM of NZVI can be enhanced with higher H₂O₂ concentrations (0.5 mM or 1 mM of H₂O₂) resulting in a pirimicarb degradation of 77.8 and 100 %, respectively. This demonstrates that different iron sources can be used for NZVI synthesis and that the subsequent degradation can be buffered by H₂O₂ concentration modifications.

3.2.2.3. Antioxidant extract selection. In order to assess the plausible synthesis of NZVI with other agro-industrial wastes, a deep comparison and characterization of the selected extracts was done and the results are explained on SM.

3.2.3. Kinetic studies

Afterwards, a kinetic study was performed in order to study the degradation behaviour and to establish the best treatment time, considering oxidation processes based on radical generation are usually quite fast [47–49].

As can be observed in Fig. 9-SM, under the optimal conditions (blueberry pruning extract with 0.02 mM H₂O₂ and 0.16 mM iron), 15 min were enough to achieve 82 % of the maximum degradation accomplished in 3 h. Indeed, Fenton-based processes do not have the potential to continue over time being almost complete after the first 30 min [47–49], although radiation application favours a slight continuity on the degradation process. Moreover, increasing the H₂O₂ concentration to 0.08 mM would have enhanced the process continuity (Fig. 5-SM).

As it can be noticed through Table 4-SM analysis, data is better adjusted in this case to a second-order kinetic. The higher degradation capacity of NZVI synthesized with blueberry pruning extract, as well as the higher pro-oxidant behaviour of this extract when compared to black tea extract (Fig. 5-SM) may favour the two-degradation pathways: Fenton reaction and active nZVI degradation. Similar results were already reported by Marcelo et al. [49] who degraded reactive blue 4 with NZVCu and the degradation profile with time was also adjusted to a second-order kinetic. The hereby attained degradation rate for pirimicarb is much better than the previously reported for the degradation of similar compounds. For instance, Chong et al. [43] attained a value of 0.006702 min⁻¹ (compared to the hereby attained 0.015 min⁻¹) for the nitrobenzene degradation with NZVZn coupled to ultrasounds. Also, Li et al. [39] tried to degrade 2,4-dichlorophenol employing higher H₂O₂ and NZVI concentrations (10 and 9 mM, respectively) and reported a kinetic constant of 0.0036 min⁻¹.

3.2.4. Validation

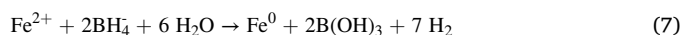
3.2.4.1. Comparison with previous studies. The attained pirimicarb degradation rates defeat previous reported results (Table 5-SM). In fact, the catalyst efficiency was calculated by the amount of pirimicarb (mg) degraded per time (min) and quantity of catalyst (g), so the data can be discussed homogeneously. As it can be seen, NZVI on this optimized photo-Fenton-NZVI process present very competitive results. Indeed, only our previous study defeats the catalyst efficiency [33]. On that case, pirimicarb degradation was much faster due to the application of an external electrochemical field at acid pH and with homogeneous Fe³⁺ as catalyst. The implementation of NZVI at a neutral pH, eliminating the need for an electric field, lowers the overall costs of application. This brings the application of this process closer to reality. On the other cases, the hereby reported data present progress towards future economically feasible usages. Hence, this catalyst efficiency (73.85 mg/g·min) defeats the data reported by Wu et al. [35]. These authors used BiVO₄ with an extremal H₂O₂ concentration (30 mM) to attain in 4 h almost complete pirimicarb degradation (10 mg/L) under simulated visible light. Their catalyst may be less photoactive than the NZVI employed in the present study as, even after having optimized the process, their pirimicarb degradation was slower under similar conditions. Similarly, Tsai et al. [34] required 24 h for 85 % degradation of a 10 mg/L pirimicarb solution under visible degradation with a Pt/AgInS₂ catalyst, which makes the process more expensive due to the usage of rare elements and the complex synthesis process. Another example was brought by Chen et al. [15] who used ZnMoO₄ to activate PMS and photodegrade pirimicarb. Nevertheless, the achieved efficiency was much lower (0.54 mg/g·min) even though they used UV radiation and higher oxidant concentrations.

Likewise, Alfaya et al. [50] got low catalytic efficiencies due to the long treatment times required to achieve complete pirimicarb degradation. Those results could have been improved by the coupling of visible radiation and the addition of an antioxidant extract, using the mine sludge they employed to generate NZVI.

Considering this is the first study when NZVI are used for pirimicarb degradation, other studies related to green-NZVI have been listed for comparison aims. Indeed, several works are based on the degradation of bromothymol blue with green-NZVI and the catalytic efficiency was extremely high. This can be related to their higher H₂O₂ concentration or the fact bromothymol blue may be easier to degrade, considering pirimicarb has been reported as a highly stable pollutant [15] (Table 5-SM). Otherwise, the other studies attained a much lower efficiency which can be related to the process synthesis. In fact, Wang et al. [51] synthesized NZVI with eucalyptus leaves, obtaining NZVI which showed a spherical shape whereas ours had a sharper structure, which may favour mass transfer and the degradation process. This difference can be caused by the lower reduction activity of the leaves extract, making the synthesis process slower [46].

3.2.4.2. Comparison with NZVI synthesized by NaBH₄ reduction. In order to assess the differences between the environmentally friendly process (reduction with blueberry pruning extract) and the typical NaBH₄ reduction for NZVI synthesis, both NZVI-extract and NZVI-NaBH₄, respectively, were compared for pirimicarb degradation (Fig. 10-SM). As it can be noticed, 20 % of degradation enhancement was attained with the green-NZVI. Thus, these particles not only are inexpensive to synthesize and environmentally friendly, but also more active. This better performance on the pirimicarb degradation can be caused by the aforementioned effect of the pro-oxidant compounds on the extract (section 3.2.2.2). Moreover, the usage of a different reducing agent may affect the physico-chemical properties of the attained NZVI. Thus a deep characterization and comparison of NZVI-extract and NZVI-NaBH₄ was carried out.

To begin with, PZC of the new NZVI-NaBH₄ particles was assessed (Fig. 11-SM). PZC was determined to be 5.64, much higher than the 3.89 of the NZVI-extract. This can be caused by the generation of hydroxide groups during the synthesis process (Eq. (7) [16].



This disparity on the PZC may cause variations on the interaction of the NZVI with pirimicarb considering its speciation with pH (Fig. 12-SM). The initial working solution had a pH of 5, consequently, pirimicarb would be both neutral and positively charged. At this working pH, NZVI-extract would be positively charged (because of their PZC to be below working pH) and NZVI-NaBH₄ may be slightly negatively charged. This can favour a significant pirimicarb adsorption into NZVI-NaBH₄, which might interfere on mass transfer and consequently degradation performance (Fig. 10-SM) [52]. Oppositely, some authors have alleged this catalyst-pollutant adsorption is beneficial to get higher degradation rates, and thus, the fact that AOPs are more efficient at acid pH can counteract this advantageous effect [53,54]. Indeed, Nguyen et al. [54] degraded more easily the positively charged crystal violet dye at acid pH although their photo-Fenton catalyst (Ag₂MoO₄/MIL-101 (Fe)/Ag composite) had a PZC of 6.4. Thus, the catalyst would be positively charged, causing catalyst-pollutant repulsion which the authors defended was favourable considering the acid environment for Fe²⁺ liberation for their photo-Fenton process.

Nevertheless, this pirimicarb adsorption into NZVI is difficult to assess, considering NZVI have themselves redox capacity for pollutants degradation. After 30 min contact of 11 mg/L of pirimicarb with 0.16 mM of NZVI-NaBH₄ or NZVI-extract, a pirimicarb reduction of, respectively 12.3 % and 5.9 % was attained, demonstrating qualitatively NZVI-NaBH₄ show some adsorption capacity, considering their catalytic performance is worse than NZVI-extract (Fig. 10-SM). Thus, the

differences on pirimicarb degradation with both NZVI can be related to their PZC.

Additionally, XPS analysis were done (Fig. 6). Survey spectra shows a higher Fe content on NZVI-NaBH₄ which is related to a clean signal which is covered by organic compounds on the NZVI-extract. Fe deconvolution show different Fe 2p peaks, related to Fe²⁺ (710.1 eV)

and Fe³⁺ (712.0 eV) [10] due to superficial passivation [55,56]. The oxygen content is higher on NZVI-extract, which is related to a higher oxidative behaviour, considering NZVI generate HO[•] and other oxygenated radicals which are anchored to the NZVI-extract surface. Indeed, O deconvolution show the main O peak on NZVI-extract is associated to organic O and it shows some adsorbed water (534.3 eV)

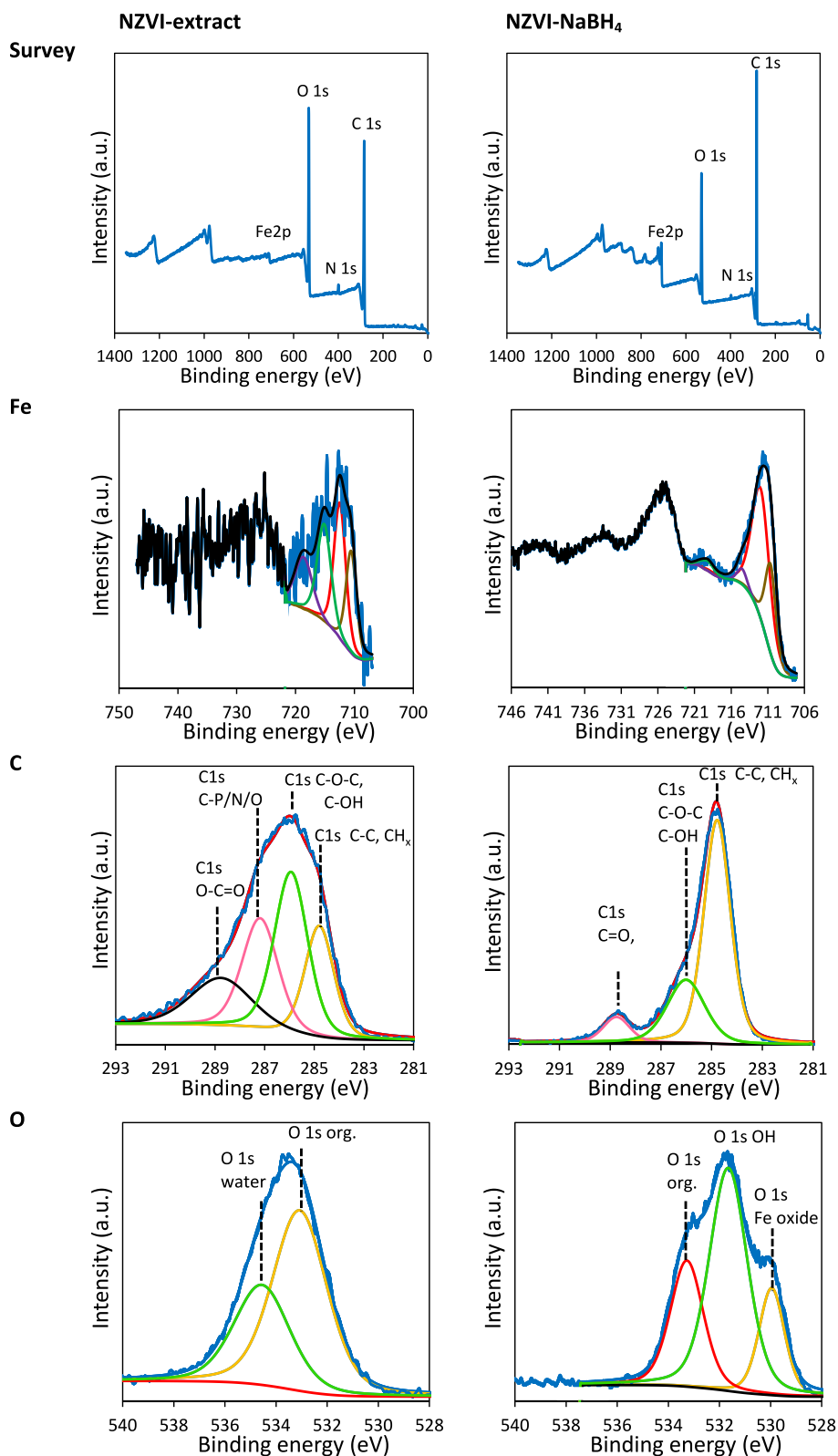


Fig. 6. XPS survey and deconvolution spectra for NZVI-extract and NZVI-NaBH₄ catalysts.

due to its positively charged surface (PZC = 3.89) which attracts water adsorption. On the case of NZVI-NaBH₄, Fe-O peak (529.9 eV) is clearly noticed because of NZVI presence [57] whereas on NZVI-extract, the organic content hinders the proper detection. Indeed, Yang et al. [56] detected this Fe-O peak after their NZVI were used, damaging the surface and favouring Fe-O detection. C deconvolution shows a richer C state mixture on the NZVI-extract surface due to the variety of organic compounds present on the antioxidant extract.

FTIR and Raman spectra were made in order to determine the different functional groups on NZVI-extract and NZVI-NaBH₄ (Fig. 7). Significant differences were found on the Raman spectra. Thus, NZVI-NaBH₄ depicted a broad peak (1,200–1,700 cm⁻¹) due to carbon-based vibrations [10]. Thick peaks at 210 and 382 cm⁻¹ indicate the presence of α-Fe₂O₃ [58].

FTIR spectra showed slight differences on both NZVI although the iron hydroxide peaks (890–1,025 cm⁻¹) [10] are noticeable on both NZVI. O–H vibrations (3400 and 1650 cm⁻¹) peaks are related to water adsorption on NZVI surface [17], which is more significant on NZVI-extract due to its acidic character (PZC = 3.89). A broader peak can be detected on NZVI-NaBH₄ between 1,300 and 1390 cm⁻¹ which is related to FeOOH vibrations [59], which is more noticeable than in NZVI-extract due to the lack of organic matter on the former.

Some structural differences can be found on SEM images (Fig. 8) when comparing both synthesis processes. NZVI-extract have a sharper structure whereas NZVI-NaBH₄ showed the previously reported spherical structure [5]. This irregular NZVI-extract structure allows the presence of more nucleation sites [14] as it can be noticed when comparing TEM images (Fig. 1 and Fig. 13-SM). Other authors have noticed the differences on the NZVI shape depending on the reducing agent [60]. The fact that NZVI-extract are more amorphous favoured the

pirimicarb degradation (Fig. 10-SM), due to the presence of more active sites [24].

Finally, UV–VIS spectra was measured, and the differences can be seen of Fig. 14-SM-A. As it can be seen, NZVI-NaBH₄ seem to have a broader NZVI peak when compared to NZVI-extract. Moreover, when comparing band gap measurement (Fig. 2-B vs Fig. 14-SM-B), NZVI-extract have several bands gaps, demonstrating its plausible activation with different wavelengths due to their defects [25] (aforementioned demonstrated on the irregular SEM images). Moreover, NZVI-extract present much higher band gaps, reaching 4.5 eV instead of the unique 1.5 eV of NZVI-NaBH₄. This is related to the fact that NZVI-extract are different than NZVI-NaBH₄ (Fig. 8) considering structural modifications affect the optical properties [60].

3.2.5. Degradation mechanism

3.2.5.1. Scavenger experiences. Scavenger reactions were carried out to establish the active species on pirimicarb degradation with the photo-Fenton-NZVI process. Thus, to the previously studied system (0.16 mM Fe and 0.02 mM H₂O₂) 2 mM of scavenger species were added, ensuring the complete trapping of the targeted substances. Thus, TEMPO was added to quench superoxide radicals, coumarin for hydroxyl radical, EDTA for the holes generated on photocatalysts [21] and sodium azide for singlet oxygen quenching [61].

The results demonstrate the main species causing pirimicarb degradation are HO[•], taking into account the 95 % detriment when these species are not available on the bulb solution (Fig. 9). This was expected, considering it is a photo-Fenton-like process, where NZVI promote its performance [2,3] and HO[•] are successfully generated. The effect of superoxide radicals (O₂^{•-}/HO₂[•]) on AOPs is also considerable [6]. On this case, 67 % of degradation reduction was observed when eliminating these oxidants from the system. This is related to the Fenton process, where the generation of O₂^{•-} following equations (8) and (9) take place due to the available H₂O₂ and the produced Fe³⁺ [3]. Moreover, NZVI can also promote the generation of superoxide radicals [4]. These species are less powerful than HO[•] although they also contribute the global Fenton performance [62].



Singlet oxygen (¹O₂) also has a role on pirimicarb degradation, demonstrating the non-radical pathway can also contribute on the pesticide degradation. These species can be generated due H₂O₂ catalytic activation [62]. Indeed, Lu et al. [55] also noticed ¹O₂ on their NZVI/H₂O₂ system when degrading the antibiotic norfloxacin.

Lastly, NZVI had a slight behaviour as photocatalyst, as it has been previously reported [57,63] and confirmed on this study (Fig. 5-SM). This fact can be established considering the trapping of the holes with EDTA caused a 15 % pirimicarb degradation detriment.

3.2.5.2. Hydroxyl radical generation. Considering the ability of NZVI to generate HO[•] that facilitate the degradation of pesticides [64] and that it has been proved HO[•] are the main degradation species (section 3.2.5.1) the quantification of this specie was conducted. As it can be seen on Fig. 15-SM, the HO[•] generation is practically instantaneous, as AOPs are extremely quick [3,62], and then the generated quantity is slightly reduced and kept constant during 3 h. This oxidant stability is due the cyclic regeneration that is caused by this photo-Fenton-NZVI process with NZVI (Eq. (1)–(4), 6 and 8) and has been previously demonstrated on the increasing pesticide degradation within time (Fig. 5-SM).

3.2.6. Degradation pathway

In order to corroborate pirimicarb degradation and to understand the degradation mechanisms, degradation by-products were measured (Table 1) and the proposed degradation pathway is presented on Fig. 16-

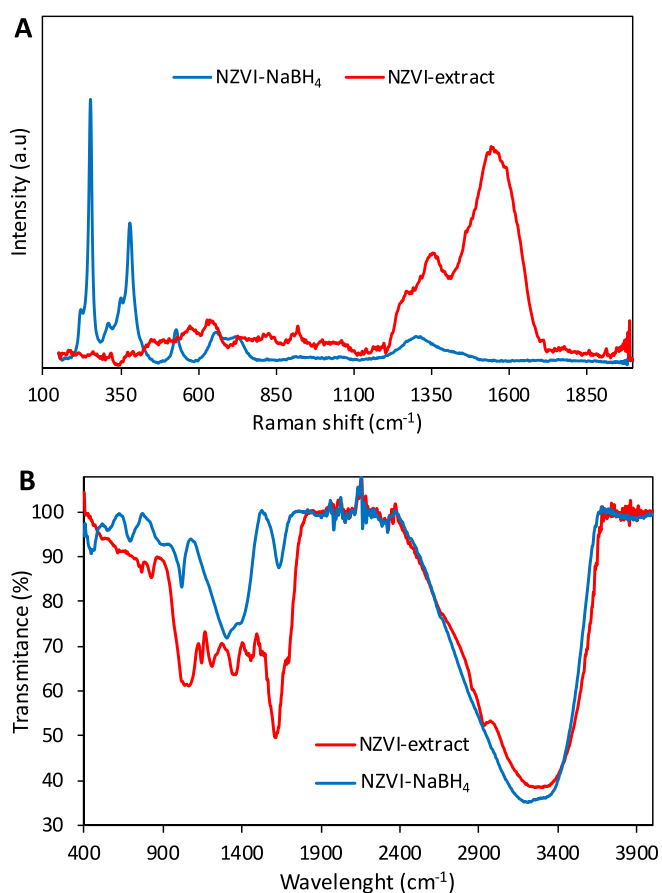


Fig. 7. Raman (A) and FTIR (B) spectra of both NZVI synthesized with blueberry pruning or NaBH₄.

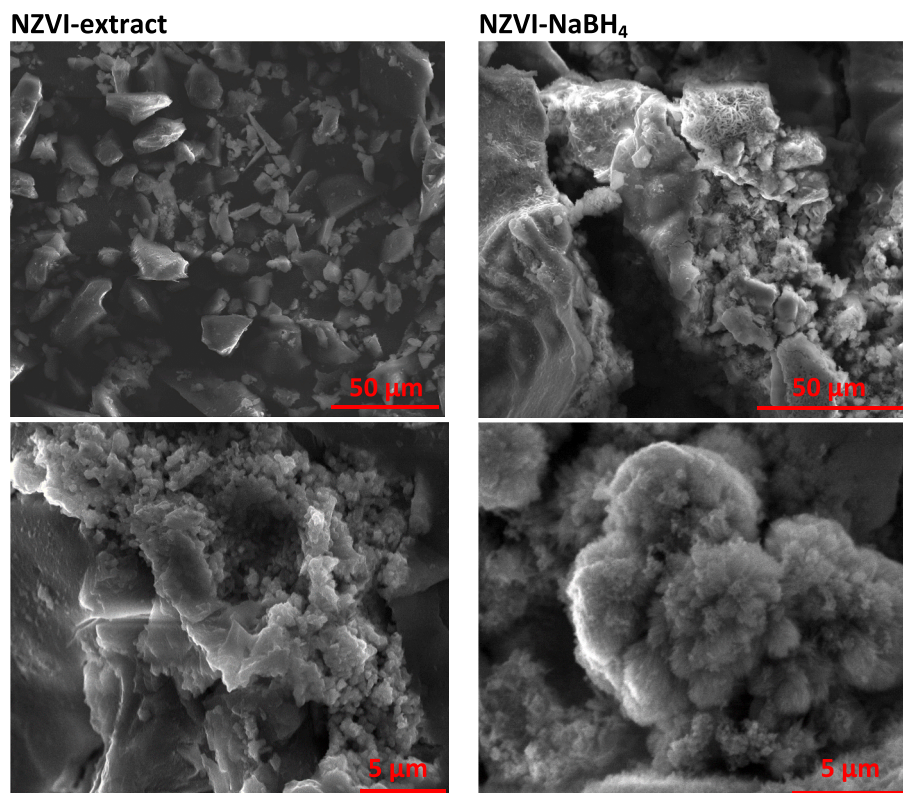


Fig. 8. SEM images of both NZVI-extract and NZVI-NaBH₄ catalysts.

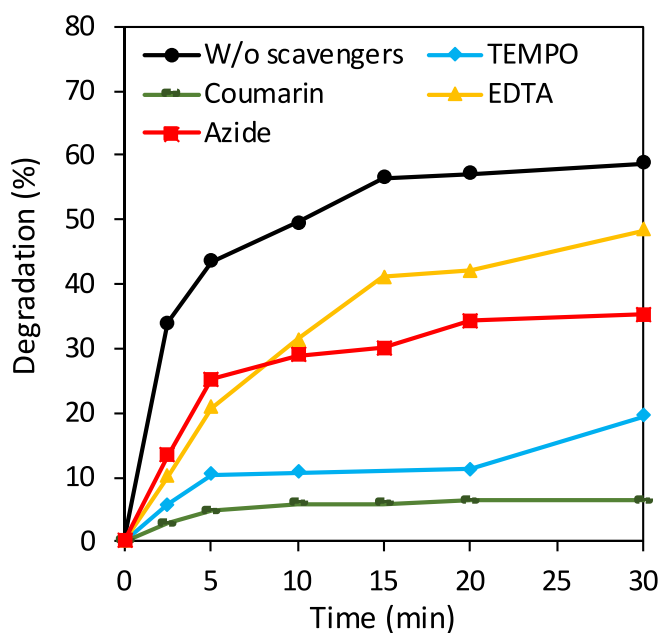


Fig. 9. Pirimicarb degradation with 0.16 mM NZVI and 0.02 mM H₂O₂ when adding different quenching reagents.

SM. Pirimicarb modification is based on the introduction of HO[•] on nucleophilic atoms (N-dimethyl group), attaining compound II [50]. The introduction of the carbonyl bond may weaken the nearby bonds, favouring the elimination of methyl and carbonyl groups, attaining compound III. From pirimicarb molecule, compound IV can be attained by the dimethylcarbamate group breakage [65]. This rupture takes place on the aldehyde bond, due to its weakness caused by the strong

electronegativity of surrounding O groups. Compound IV can suffer N-dealkylation (compound V) [50]. After this, subsequent breakages and even radical recombination produce compound VI and the carboxylic acids detected by HPLC-DAD (Fig. 16-SM), demonstrating the successful pirimicarb degradation.

3.2.7. Catalyst recycling

The reusability of the synthesized particles was done by the subsequent addition of blueberry pruning extract and 0.02 mM H₂O₂ (Fig. 17-SM). On the second batch a slight degradation increase could be noticed which can be related to the iron leaching (0.11 ng/L) favouring homogeneous photo-Fenton process and the reduction of the oxidized iron species generated during the first batch. However, as the subsequent batches took place, the degradation performance decreases, demonstrating the NZVI are spent and maybe agglomerated, impeding their activity [23]. In fact, in these cases iron leaching was below detection limit. Considering the inefficient NZVI reusability and the small initial iron quantity added on this study, new iron solution should be added in each batch (section 3.2.8).

3.2.8. Inlet effluent

The pollutant degradation in the presence of other matrixes was tested (Table 6-SM). As expected, the degradation process was less efficient due to matrix interferences. Indeed, the real wastewater treated has a conductivity of 1 mS/cm and a total solid content of 19 mg/L. In addition, tap water and real wastewater have several ions, such as Ca²⁺, Mg²⁺, Na⁺, K⁺, HCO₃⁻, Cl⁻ and SO₄²⁻, whose presence may prevent the contact of the organic matter with NZVI and iron hydroxides [1]. Nevertheless, those ions overcome the slight toxicity of NZVI due to electrostatic repulsion of the NZVI with microorganisms in those high conductivity effluents [67].

In order to increase the process performance, a subsequent addition of iron solution (0.16 mM), blueberry pruning extract and 0.02 mM H₂O₂, was done. This was based on the subsequent addition of fresh

reagents on other oxidative process, such as the Fenton and photo-Fenton processes. Indeed, Demir-Duz et al. [44] have previously reported that a new H_2O_2 addition after the whole photo-Fenton process enhanced by 27 % the difficult degradation of real refinery wastewater. These authors mentioned that some compounds present on real wastewater can scavenge H_2O_2 and make this subsequent addition necessary. Other photo-Fenton studies have evaluated the effect of a new addition of iron, and for Araña et al. [68] it was an alternative to reduce drastically the treatment time for the photo-Fenton degradation of ethylene glycol.

In the present study, the reported approach reveals to be an efficient process. In fact, after the subsequent addition of reagents, the pirimicarb degradation was considerably enhanced and after the third addition, pirimicarb degradation surpassed 75 % (Table 6-SM) in all the matrixes. As the degradation cycles pass, the degradation process seems easier which can be related to the easier degradation of the pirimicarb by-products, such as carboxylic acids or the opened pirimicarb ring (Fig. 16-SM). Another alternative when working with more complex effluents could be the increase of H_2O_2 concentration as it was demonstrated in this study (section 3.2.2.1) and reported in another AOPs, such as the photo-Fenton degradation performed by Araña et al. [68] who established a ratio between the H_2O_2 addition and the total organic content (TOC) of the effluent (8.5 mol H_2O_2 /mol TOC). In fact, in this study the ratio is widely lower (0.003) considering the selected H_2O_2 concentration (0.02 mM) and the TOC of the initial effluent (6.3 mg/L, when using distilled water). Moreover, other approaches have been reported to enhance NZVI performance, such as the usage of ultrasounds which not only favours the generation of radicals due to cavitation but also favours the dispersion of NZVI [43]. In any case, the successful degradation of pirimicarb in different matrixes is unlikely to be related to the iron leaching as it was found to be below 3.5 % in every batch, reaching a maximum of 0.31 ng/L on the third batch of distilled water. The leaching was even lower when working with tap water and real wastewater (0.30 and 0.28, respectively), fact which can be attributed to metal complexation due to the salts and organic matter present on these matrixes. In any case, these values are far below the allowed liberation limits (2 mg/L) [69], making this process future usage feasible.

In future research, all the referred alternatives might be considered for the successful treatment of real matrixes in a potential scale-up. It is worth mentioning that the usage of higher H_2O_2 concentrations is a quick process for attaining complete pirimicarb degradation, although it was demonstrated that the subsequent addition of NZVI, antioxidant extract and H_2O_2 favours the generation of more oxidants and thus the overall H_2O_2 concentration required is much smaller. Indeed, 0.04 mM of H_2O_2 have been required for complete pirimicarb degradation (2 batches) in the Milli-Q matrix (Table 6-SM), whereas 0.08 mM were required for attaining the same degradation in an individual spick (Fig. 4).

4. Conclusions

Several processes based on NZVI have been assessed. Under simulated solar irradiation, *in situ* synthesized NZVI have better performance than the widely reported homogeneous photo-Fenton process. Moreover, the NZVI synthesis have been assessed with different natural extracts (black tea, blueberry and vineyard pruning, and algae) and even with traditional $NaBH_4$. From the tested extracts, only brown algae demonstrated to be not suitable for pirimicarb degradation due to its low reduction capability. Small iron quantities were needed (0.16 mM) for attaining the highest pirimicarb removal rate. Concerning the H_2O_2 addition, it is proportional to the degradation degree, although 0.02 mM was fixed as working value to avoid an excess of environmentally unfriendly reagents on the bulb system. Pirimicarb by-products were detected, demonstrating the successful degradation of the pesticide. The NZVI reuse showed some limitations which can be overlooked considering the low NZVI concentration used and the inexpensive and green

synthesis process required for their synthesis. As expected, working with more complex matrixes (tap water or real wastewater) reduces the process performance, although it can be overcome by the sequential addition of fresh reagents. Thus, the proposed process has the malleability for being adapted to different inlet conditions. This process fits within the circular economy as it favours the degradation of an emerging pollutant with the usage of solar radiation and real wastes which would be, otherwise, landfilled.

Funding

This work was supported by UIDB/50006/2020 and UIDP/50006/2020 by the Fundação para a Ciência e a Tecnologia (FCT)/Ministério da Ciência, Tecnologia e Ensino Superior (MCTES) through national funds. The researcher Aida M. Díez is grateful to Xunta de Galicia for the financial support obtained (ED481D-2023/015) as well as to Iacobus program under European Union funds. This work was supported by Deputación Provincial de Pontevedra. This work has been funded by MCIN/AEI/10.13039/501100011033 and European Union Next Generation funds EU/PRTR (PDC2021-121394-I00). Manuela M. Moreira (CEECIND/02702/2017) is grateful for her contract financed by FCT/MCTES—CEEC Individual Program Contract and to REQUIMTE/LAQV. This research was funded through the join 2019–2020 Biodiversa & Water JPI joint call for research proposals, under the BiodivRestore ERA-Net COFUND programme. Project PCI2022-132941 funded by MCIN/AEI /<https://doi.org/10.13039/501100011033> and European Union Next Generation EU/PRTR. Funding for open access charge: Universidade de Vigo/CISUG.

CRediT authorship contribution statement

A.M. Díez: . **Manuela M. Moreira:** Investigation, Methodology, Software, Visualization. **M. Pazos:** Funding acquisition, Project administration, Supervision, Writing – review & editing. **M.A. Sanromán:** . **T. Albergaria:** Conceptualization, Funding acquisition, Project administration, Supervision, Writing – review & editing. **C. Delerue-Matos:** Conceptualization, Funding acquisition, Project administration, Writing – review & editing.

Declaration of competing interest

The authors declare that they have no known competing financial interests or personal relationships that could have appeared to influence the work reported in this paper.

Data availability

Data will be made available on request.

Appendix A. Supplementary material

Supplementary data to this article can be found online at <https://doi.org/10.1016/j.seppur.2023.126179>.

References

- [1] H. Li, X. Li, J. Long, K. Li, Y. Chen, J. Jiang, X. Chen, P. Zhang, Oxidation and removal of thallium and organics from wastewater using a zero-valent-iron-based Fenton-like technique, *J. Clean. Prod.* 221 (2019) 89–97, <https://doi.org/10.1016/j.jclepro.2019.02.205>.
- [2] W. Zhang, H. Gao, J. He, P. Yang, D. Wang, T. Ma, H. Xia, X. Xu, Removal of norfloxacin using coupled synthesized nanoscale zero-valent iron (nZVI) with H_2O_2 system: Optimization of operating conditions and degradation pathway, *Sep. Purif. Technol.* 172 (2017) 158–167, <https://doi.org/10.1016/j.seppur.2016.08.008>.
- [3] J.J. Pignatello, E. Oliveros, A. MacKay, Advanced oxidation processes for organic contaminant destruction based on the Fenton reaction and related chemistry, *Crit. Rev. Environ. Sci. Technol.* 36 (2006) 1–84, <https://doi.org/10.1080/10643380500326564>.
- [4] C. Duca, H. Bogo, M.I. Litter, E.S. Román, Heterogeneous photo-Fenton process with zerovalent iron nanoparticles for degradation of toluene in aqueous solution,

- Catal. Commun. 183 (2023) 106767, <https://doi.org/10.1016/j.catcom.2023.106767>.
- [5] C. Lin, S. Hsu, Performance of nZVI/H₂O₂ process in degrading polyvinyl alcohol in aqueous solutions, Sep. Purif. Technol. 203 (2018) 111–116, <https://doi.org/10.1016/j.seppur.2018.03.041>.
- [6] M.R. Samarghandi, A. Dargahi, H.Z. Nasab, E. Ghahramani, S. Salehi, Degradation of azo dye Acid Red 14 (AR14) from aqueous solution using H₂O₂/nZVI and S2O8²⁻/nZVI processes in the presence of UV irradiation, Water Environ. Res. 92 (2020) 1173–1183, <https://doi.org/10.1002/wer.1312>.
- [7] F.M. Ertosun, K. Cellat, O. Eren, S. Gul, E. Kusvuran, F. Sen, Comparison of nanoscale zero-valent iron, fenton, and photo-fenton processes for degradation of pesticide 2,4-dichlorophenoxyacetic acid in aqueous solution, Sn Applied Sciences 1 (2019) 1491, <https://doi.org/10.1007/s42452-019-1554-5>.
- [8] R. Yuvakkumar, V. Elango, V. Rajendran, N. Kannan, Preparation and characterization of zero valent iron nanoparticles, Dig. J. Nanomat. Biostr. 6 (2011) 1771–1776.
- [9] K. Manquian-Cerda, E. Cruces, M.A. Rubio, C. Reyes, N. Arancibia-Miranda, Preparation of nanoscale iron (oxide, oxyhydroxides and zero-valent) particles derived from blueberries: Reactivity, characterization and removal mechanism of arsenate, Ecotoxicol. Environ. Saf. 145 (2017) 69–77, <https://doi.org/10.1016/j.ecoenv.2017.07.004>.
- [10] C. Zhang, D. Wang, Q. Liu, J. Tang, Ligand-citric acid enhanced in-situ ROS generation by GBc/nZVI to promote the aerobic degradation of adsorbed 2,4-dichlorophenol, Chem. Eng. J. 477 (2023) 147126, <https://doi.org/10.1016/j.cej.2023.147126>.
- [11] S. Machado, J.G. Pacheco, H.P.A. Nows, J.T. Albergaria, C. Delerue-Matos, Characterization of green zero-valent iron nanoparticles produced with tree leaf extracts, Sci. Total Environ. 533 (2015) 76–81, <https://doi.org/10.1016/j.scitotenv.2015.06.091>.
- [12] B. Desalegn, M. Megharaj, Z. Chen, R. Naidu, Green synthesis of zero valent iron nanoparticle using mango peel extract and surface characterization using XPS and GC-MS, Heliyon 5 (2019), <https://doi.org/10.1016/j.heliyon.2019.e01750>.
- [13] C.D. Raman, K. Sellappa, M. Mkandawire, Facile one step green synthesis of iron nanoparticles using grape leaves extract: textile dye decolorization and wastewater treatment, Water Sci. Technol. 83 (2021) 2242–2258.
- [14] M.V. Arularasu, J. Devakumar, T.V. Rajendran, An innovative approach for green synthesis of iron oxide nanoparticles: Characterization and its photocatalytic activity, Polyhedron 156 (2018) 279–290, <https://doi.org/10.1016/j.poly.2018.09.036>.
- [15] C. Chen, H. Fan, J. Shaya, Y. Chang, V.B. Golovko, O. Toulemonde, C. Huang, Y. Song, C. Lu, Accelerated ZnMoO₄ photocatalytic degradation of pirimicarb under UV light mediated by peroxymonosulfate, Appl. Organomet. Chem. 33 (2019) e5113.
- [16] T. Bao, M.M. Dantie, A. Hosseinzadeh, R.L. Frost, Z.M. Yu, J. Jin, K. Wu, Catalytic degradation of P-chlorophenol by muscovite-supported nano zero valent iron composite: Synthesis, characterization, and mechanism studies, Appl. Clay Sci. 195 (2020) 105735, <https://doi.org/10.1016/j.clay.2020.105735>.
- [17] Y. Bagbi, A. Sarswat, S. Tiwari, D. Mohan, A. Pandey, P.R. Solanki, Synthesis of l-cysteine stabilized zero-valent iron (nZVI) nanoparticles for lead remediation from water, Environ. Nanotechnol. Monit. Manage. 7 (2017) 34–45, <https://doi.org/10.1016/j.enmm.2016.11.008>.
- [18] A.O. Dada, F.A. Adekola, E.O. Odeunmi, Synthesis and characterization of iron nanoparticles and its ash rice husk supported nanocomposite (2014).
- [19] M.A.I. Ahmed, N.S. Khalil, T.A.E.A.E. Rahman, Carbamate pesticide residue analysis of Potato tuber samples using high-performance liquid chromatography (HPLC), Journal of Environmental Chemistry and Ecotoxicology 6 (2014) 1–5, <https://doi.org/10.5897/JECE2013.0309>.
- [20] M.M. Moreira, F. Rodrigues, O. Dorosh, D. Pinto, P.C. Costa, J. Svarc-Gajic, C. Delerue-Matos, Vine-Canes as a Source of Value-Added Compounds for Cosmetic Formulations, Molecules 25 (2020) 2969, <https://doi.org/10.3390/molecules25132969>.
- [21] A. Torres-Pinto, A.M. Díez, C.G. Silva, J.L. Faria, M.Á. Sanromán, A.M.T. Silva, M. Pazos, Photoelectrocatalytic degradation of pharmaceuticals promoted by a metal-free g-C₃N₄ catalyst, Chem. Eng. J. 476 (2023) 146761, <https://doi.org/10.1016/j.cej.2023.146761>.
- [22] M. Tokumura, R. Morito, R. Hatayama, Y. Kawase, Iron redox cycling in hydroxyl radical generation during the photo-Fenton oxidative degradation: Dynamic change of hydroxyl radical concentration, Appl Catal B 106 (2011) 565–576, <https://doi.org/10.1016/j.apcatb.2011.06.017>.
- [23] Y. Hwang, Y. Lee, P.D. Mines, Y.S. Huh, H.R. Andersen, Nanoscale zero-valent iron (nZVI) synthesis in a Mg-aminoclay solution exhibits increased stability and reactivity for reductive decontamination, Applied Catalysis B-Environmental 147 (2014) 748–755, <https://doi.org/10.1016/j.apcatb.2013.10.017>.
- [24] S. Panić, M. Petronijević, J. Vukmirović, N. Grba, S. Savić, Green Synthesis of Nanoscale Zero-Valent Iron Aggregates for Catalytic Degradation of Textile Dyes, Catal. Lett. (2023) 1–15.
- [25] P.K. Sharma, O.P. Pandey, Synthesis and catalytic study of CeO₂ heterostructures with (Zn_{0.003-x}Cd_x)SO₄ for the removal of crystal violet dye, Physica B: Condensed Matter 631 (2022) 413702, <https://doi.org/10.1016/j.physb.2022.413702>.
- [26] M. Pirsahab, S. Moradi, M. Shahlaei, X. Wang, N. Farhadian, A new composite of nano zero-valent iron encapsulated in carbon dots for oxidative removal of bio-refractory antibiotics from water, J. Clean. Prod. 209 (2019) 1523–1532, <https://doi.org/10.1016/j.jclepro.2018.11.175>.
- [27] G. Zhou, W. Li, C. He, X. Liu, R. Ding, Y. Wang, Y. Mu, Enhanced hydrodeiodination of iodinated contrast medium by sulfide-modified nano-sized zero-valent iron: Kinetics, mechanisms and application prospects, Chem. Eng. J. 401 (2020) 126050, <https://doi.org/10.1016/j.cej.2020.126050>.
- [28] F. Meng, J. Xu, H. Dai, Y. Yu, D. Lin, Even Incorporation of Nitrogen into FeO Nanoparticles as Crystalline Fe₄N for Efficient and Selective Trichloroethylene Degradation, Environ. Sci. Technol. 56 (2022) 4489–4497.
- [29] J. Xiao, R. Li, H. Dong, Y. Li, L. Li, S. Xiao, Z. Jin, Activation of sulfite via zero-valent iron-manganese bimetallic nanomaterials for enhanced sulfamethazine removal in aqueous solution: Key roles of Fe/Mn molar ratio and solution pH, Sep. Purif. Technol. 297 (2022) 121479, <https://doi.org/10.1016/j.seppur.2022.121479>.
- [30] S. Nobsathian, P. Tuchinda, P. Sobhon, Y. Tinikul, J. Poljaroen, R. Tinikul, M. Sroyraya, T. Poomton, S. Chaichotranunt, An antioxidant activity of the whole body of *Holothuria scabra*, Chemical and Biological Technologies in Agriculture 4 (2017) 4, <https://doi.org/10.1186/s40538-017-0087-7>.
- [31] S. Machado, J.P. Grosso, H.P.A. Nows, J.T. Albergaria, C. Delerue-Matos, Utilization of food industry wastes for the production of zero-valent iron nanoparticles, Sci. Total Environ. 496 (2014) 233–240, <https://doi.org/10.1016/j.scitotenv.2014.07.058>.
- [32] H. Dihinia, S. Pathak, L. Lalmalsawdawngliani, D. Tiwari, D. Kim, A sustainable solution for diclofenac degradation from water by heterojunction bimetallic nanocatalyst, J. Taiwan Inst. Chem. Eng. (2023) 105096, <https://doi.org/10.1016/j.jtice.2023.105096>.
- [33] A.M. Díez, M.A. Sanromán, M. Pazos, Sequential two-column electro-Fenton-photolytic reactor for the treatment of winery wastewater, Environ. Sci. Pollut. Res. (2016) 1–15, <https://doi.org/10.1007/s11356-016-7937-x>.
- [34] H. Tsai, J. Shaya, S. Tesana, V.B. Golovko, S. Wang, Y. Liao, C. Lu, C. Chen, Visible-light driven photocatalytic degradation of pirimicarb by Pt-doped AgInS₂ nanoparticles, Catalysts 10 (2020) 857.
- [35] Y. Wu, C. Chen, Y. Huang, W. Lin, Y. Yen, C. Lu, Pirimicarb degradation by BiVO₄ photocatalysis: Parameter and reaction pathway investigations, Sep. Sci. Technol. 51 (2016) 2284–2296, <https://doi.org/10.1080/01496395.2016.1202279>.
- [36] I.A. Ndanusa, B.O. Aderemi, A. Hamza, D.B. Hassan, Application of Response Surface Methodology for Optimization of Phenol Degradation in Photo-Fenton process by Nano Zero Valent Iron Composite (2022).
- [37] W. Moyo, T.T. Nkambule, Removal of natural organic matter fractions by adsorptive asymmetric ceramic membrane functionalized with in situ phytochemical nanoscale zero valent iron: Performance and Fenton cleaning strategy, Environ. Prog. Sustain. Energy (2022) e14053.
- [38] S. Le, A. Israpanich, T. Phenrat, Using sequential H₂O₂ addition to sustain 1,2-dichloroethane detoxification by a nanoscale zerovalent iron-induced Fenton's system at a natural pH, Chemosphere 305 (2022) 135376, <https://doi.org/10.1016/j.chemosphere.2022.135376>.
- [39] R. Li, Y. Gao, X. Jin, Z. Chen, M. Megharaj, R. Naidu, Fenton-like oxidation of 2,4-DCP in aqueous solution using iron-based nanoparticles as the heterogeneous catalyst, J. Colloid Interface Sci. 438 (2015) 87–93, <https://doi.org/10.1016/j.jcis.2014.09.082>.
- [40] Y. Li, Y. Zhang, G. Xia, J. Zhan, G. Yu, Y. Wang, Evaluation of the technoeconomic feasibility of electrochemical hydrogen peroxide production for decentralized water treatment, Front. Environ. Sci. Eng 15 (1) (2021) 1–15.
- [41] K. Vidot, C. Maury, R. Siret, M. Lahaye, Phenolic compounds limit or promote oxidative degradation of pectin related to iron-H₂O₂ limits, Lwt-Food Science and Technology 125 (2020) 109324, <https://doi.org/10.1016/j.lwt.2020.109324>.
- [42] G.H. Qasim, H. Fareed, M. Lee, W. Lee, S. Han, Aqueous monomethylmercury degradation using nanoscale zero-valent iron through oxidative demethylation and reductive isolation, J. Hazard. Mater. 435 (2022) 128990, <https://doi.org/10.1016/j.jhazmat.2022.128990>.
- [43] S. Chong, Y. Song, H. Zhao, G. Zhang, Enhanced degradation of nitrobenzene by combined ultrasonic irradiation and a zero-valent zinc catalyst, Desalin. Water Treat. 57 (2016) 23856–23863, <https://doi.org/10.1080/19443994.2016.1138887>.
- [44] H. Demir-Duz, O. Ayyildiz, A.S. Akturk, M.G. Alvarez, S. Contreras, Approaching zero discharge concept in refineries by solar-assisted photo-Fenton and photocatalysis processes, Applied Catalysis B-Environmental 248 (2019) 341–348, <https://doi.org/10.1016/j.apcatb.2019.02.026>.
- [45] K. Marquez, D. Contreras, P. Salgado, C. Mardones, Production of hydroxyl radicals and their relationship with phenolic compounds in white wines, Food Chem. 271 (2019) 80–86, <https://doi.org/10.1016/j.foodchem.2018.07.165>.
- [46] J. Yu, X. Zhang, R. Ma, Y. Du, X. Zhao, S. Zuo, K. Dong, R. Wang, Y. Zhang, Y. Gu, Degradation of 2, 4-Dichlorophenol Through Fenton Process Catalyzed by Nanoscale Zero-Valent Iron Supported by Biochar, Water Air Soil Pollut. 234 (2023) 404.
- [47] A.M. Soubh, M. Baghdadi, M.A. Abdoli, B. Aminzadeh, Activation of Persulfate Using an Industrial Iron-Rich Sludge as an Efficient Nanocatalyst for Landfill Leachate Treatment, Catalysts 8 (2018) 218, <https://doi.org/10.3390/catal8050218>.
- [48] M.A. Tony, L. Lin, Iron recovery from acid mine drainage sludge as Fenton source for municipal wastewater treatment, Int. J. Environ. Anal. Chem. (2020)10.1080/03067319.2020.1734196.
- [49] C.R. Marcelo, G.A. Puiatti, M.A. Nascimento, A.F. Oliveira, R.P. Lopes, Degradation of the Reactive Blue 4 Dye in Aqueous Solution Using Zero-Valent Copper Nanoparticles, J. Nanomater. 2018 (2018) 4642038, <https://doi.org/10.1155/2018/4642038>.
- [50] E. Alfaya, O. Iglesias, M. Pazos, M. Angeles Sanroman, Environmental application of an industrial waste as catalyst for the electro-Fenton-like treatment of organic pollutants, RSC Adv. 5 (2015) 14416–14424, <https://doi.org/10.1039/c4ra15934a>.

- [51] T. Wang, J. Lin, Z. Chen, M. Megharaj, R. Naidu, Green synthesized iron nanoparticles by green tea and eucalyptus leaves extracts used for removal of nitrate in aqueous solution, *J. Clean. Prod.* 83 (2014) 413–419, <https://doi.org/10.1016/j.jclepro.2014.07.006>.
- [52] W. Zhang, P. Gago-Ferrero, Q. Gao, L. Ahrens, K. Blum, A. Rostvall, B. Björleinius, P.L. Andersson, K. Wiberg, P. Haglund, G. Renman, Evaluation of five filter media in column experiment on the removal of selected organic micropollutants and phosphorus from household wastewater, *J. Environ. Manage.* 246 (2019) 920–928, <https://doi.org/10.1016/j.jenvman.2019.05.137>.
- [53] F.J. Beltrán, P. Pocostales, P. Alvarez, A. Oropesa, Diclofenac removal from water with ozone and activated carbon, *J. Hazard. Mater.* 163 (2009) 768–776, <https://doi.org/10.1016/j.jhazmat.2008.07.033>.
- [54] H.T. Nguyen, M.T. Truong, V. Doan, T.L.H. Nguyen, V.H. Hoang, V.A. Tran, A. Nguyen, V.T. Le, Constructing a novel Ag₂MoO₄/ML-101(Fe)/Ag composite for efficient crystal violet degradation via photo-Fenton-like process, *Chem. Eng. Sci.* 284 (2024) 119487, <https://doi.org/10.1016/j.ces.2023.119487>.
- [55] B. Lu, Z. Fang, P.E. Tsang, J. Wu, Effect and mechanism of norfloxacin removal by guava leaf extract in the ZVI/H₂O₂ system, *Chemosphere* 316 (2023) 137801, <https://doi.org/10.1016/j.chemosphere.2023.137801>.
- [56] S. Yang, J. Tang, X. Zhang, A. Zhang, Degradation of refractory organic matter in MBR effluent from treating landfill leachate by the UV-nZVI-H₂O₂ system, *Environ. Sci. Pollut. Res.* 30 (2023) 50295–50308.
- [57] A. Sinharoy, P. Uddandarao, Zero-Valent Nanomaterials for Wastewater Treatment, in: *Advanced Application of Nanotechnology to Industrial Wastewater*, Springer, 2023, pp. 53–73.
- [58] X. Li, M. Gao, Y. Huo, H. Liu, J. Li, T. Huang, R. Ye, W. Li, Impacts of shell structure on nitrate-reduction activity and air stability of nanoscale zero-valent iron, *Environ. Sci. Pollut. Res.* 29 (2022) 80683–80692.
- [59] E.M. Abd El-Monaem, A.M. Omer, G.M. El-Subruiti, M.S. Mohy-Eldin, A. S. Eltaweil, Zero-valent iron supported-lemon derived biochar for ultra-fast adsorption of methylene blue, *Biomass Convers. Biorefin.* (2022) 1–13.
- [60] T. Kumari, D. Phogat, V. Shukla, Exploring the multipotentiality of plant extracts for the green synthesis of iron nanoparticles: A study of adsorption capacity and dye degradation efficiency, *Environ. Res.* 229 (2023) 116025, <https://doi.org/10.1016/j.envres.2023.116025>.
- [61] E. Brillas, Progress of antibiotics removal from synthetic and real waters and wastewaters by persulfate-based advanced oxidation processes, *J. Environ. Chem. Eng.* 11 (2023) 111303, <https://doi.org/10.1016/j.jece.2023.111303>.
- [62] Z. Xie, C. He, D. Pei, Y. Dong, S. Yang, Z. Xiong, P. Zhou, Z. Pan, G. Yao, B. Lai, Review of characteristics, generation pathways and detection methods of singlet oxygen generated in advanced oxidation processes (AOPs), *Chem. Eng. J.* 468 (2023) 143778, <https://doi.org/10.1016/j.cej.2023.143778>.
- [63] K. Bhuvaneshwari, S. Radha, B.S. Sreeja, G. Palanisamy, T. Pazhanivel, Study of the morphological, structural and photophysical properties of surfactant modified nano-zero valent iron: electrochemical determination of metal ions and photocatalytic degradation of organic dye, *J. Mater. Sci. : Mater. Electron.* 34 (2023) 277.
- [64] T. Maezono, M. Tokumura, M. Sekine, Y. Kawase, Hydroxyl radical concentration profile in photo-Fenton oxidation process: Generation and consumption of hydroxyl radicals during the discoloration of azo-dye Orange II, *Chemosphere* 82 (2011) 1422–1430, <https://doi.org/10.1016/j.chemosphere.2010.11.052>.
- [65] J. Fenoll, I. Garrido, P. Hellín, P. Flores, N. Vela, S. Navarro, Photocatalytic oxidation of pirimicarb in aqueous slurries containing binary and ternary oxides of zinc and titanium, *J. Photochem. Photobiol. a.* 298 (2015) 24–32, <https://doi.org/10.1016/j.jphotochem.2014.10.014>.
- [66] T. Chen, F. Fu, Z. Chen, D. Li, L. Zhang, G. Chen, Study on the photodegradation and microbiological degradation of pirimicarb insecticide by using liquid chromatography coupled with ion-trap mass spectrometry, *J. Chromatogr. A* 1216 (2009) 3217–3222, <https://doi.org/10.1016/j.chroma.2009.02.022>.
- [67] Y. Cheng, H. Dong, Y. Lu, K. Hou, Y. Wang, Q. Ning, L. Li, B. Wang, L. Zhang, G. Zeng, Toxicity of sulfide-modified nanoscale zero-valent iron to *Escherichia coli* in aqueous solutions, *Chemosphere* 220 (2019) 523–530, <https://doi.org/10.1016/j.chemosphere.2018.12.159>.
- [68] J. Arana, J.A. Ortega Mendez, J.A. Herrera Melian, J.M. Dona Rodriguez, O. Gonzalez Diaz, J. Perez Pena, Thermal effect of carboxylic acids in the degradation by photo-Fenton of high concentrations of ethylene glycol, *Applied Catalysis B-Environmental* 113 (2012) 107–115, [10.1016/j.apcatb.2011.11.025](https://doi.org/10.1016/j.apcatb.2011.11.025).
- [69] A. Torres-Pinto, M.J. Sampaio, J. Teixo, C.G. Silva, J.L. Faria, A.M.T. Silva, Photo-Fenton degradation assisted by in situ generation of hydrogen peroxide using a carbon nitride photocatalyst, *J. Water Process Eng.* 37 (2020) 101467, <https://doi.org/10.1016/j.jwpe.2020.101467>.